Non thermal plasma assisted catalysis of methanol oxidation on Mn, Ce and Cu oxides supported on γ-Al 2 O 3

Caroline Norsic, Jean-Michel Tatibouet, Catherine Batiot-Dupeyrat, Elodie Fourre

Non thermal plasma assisted catalysis of methanol oxidation on Mn, Ce and Cu oxides supported on γ-Al_2O_3

Caroline Norsic[a], Jean-Michel Tatibouët[a], Catherine Batiot-Dupeyrat[a], Elodie Fourré[a]

[a] Institut de Chimie des Milieux et Matériaux de Poitiers (IC2MP), UMR CNRS 7285
Université de Poitiers, Ecole Nationale Supérieure d'Ingénieurs de Poitiers (ENSIP)
1, rue marcel Doré, TSA 41105, 86073 Poitiers cedex 9 (France)

Corresponding author: elodie.fourre@univ-poitiers.fr

Other authors: caroline.norsic@univ-poitiers.fr
jean.michel.tatibouet@univ-poitiers.fr
Catherine.batiot.dupeyrat@univ-poitiers.fr

Keywords

Non thermal plasma, methanol, oxidation, metal oxide, TPR, ozone

Highlights

- A plasma reactor with an elaborated configuration was developed
- Single plasma led to methanol conversion of 75 % at 25 ppm initial concentration
- $MnO_2/CeO_2/ Al_2O_3$ and $MnO_2/CuO/Al_2O_3$ catalysts presented the best activities
- The reactor configuration and catalyst support may be extrapolated to larger scale

Abstract

A non thermal plasma reactor coupled with different metal oxide based catalysts (MnO_2, CeO_2, CuO, MnO_2-CeO_2, MnO_2-CuO supported on Al_2O_3) has been developed for the decomposition of methanol at low concentration (25-150 ppm) and low residence time (0.36 s) in an air flow. The geometry of the reactor developed in this study led to the formation of a surface plasma that presented high energetic efficiency since 75 % methanol conversion was reached with a concentration of 25 ppm of methanol at an energy density of 20 $J.L^{-1}$ in a single plasma configuration. The methanol conversion was improved when a catalyst was placed beyond the discharge. Apart from CO_2, secondary products were identified as formaldehyde, methyl formate, methylal, CO and ozone. The influence of the methanol concentration, energy density and metal oxide catalyst composition on the methanol conversion, by-products selectivities and ozone formation were studied. The best methanol conversion and lower ozone residual concentration were obtained with bimetallic oxides $MnO_2/CuO/Al_2O_3$ and $MnO_2/CeO_2/Al_2O_3$. A kinetic model and reaction mechanisms were proposed for methanol decomposition without catalyst, building on the work carried out in diverse publications.

1. Introduction

Considering the prevailing problematics regarding air quality (and consecutive impact on health), global warming and rising worldwide demand in energy, the use of viable technologies allowing air purification at lowest energy costs appears as an undeniable solution to overcome these environmental issues. Within the variety of accessible new technologies, non thermal atmospheric plasma (NTAP) is now recognized as an efficient, low cost process which has led to a large amount of research on numerous applications (energy, depollution, biomedical, surface functionalization, to name a few), published work and reviews [1-8]. Within the diversity of non thermal plasma configurations [3], dielectric barrier discharge (DBD) plasma has reached a place of interest mainly due to its flexibility and energy efficiency. DBD plasma is an ionized gas that can be obtained by applying a high difference of potential between two electrodes isolated from each other by a dielectric. Under a gaseous atmosphere, electrons are accelerated by an electric field and collide with neutral molecules in the gas phase which generates highly active species (atoms, ions, electrons, free radicals, photons, etc.). In such a case (non-equilibrium plasma), the temperature of electrons is much higher than that of the gas so that the process can take place at near ambient temperature. It can be recalled that non thermal plasma first applications concerned the production of ozone and soon after water purification [4-5]. Consequently, for the purpose of improving air quality, research on gas treatment and volatile organic compounds (VOCs) removal were largely studied [6-10]. It was also demonstrated that the presence of a catalyst within a plasma discharge resulted in a synergistic effect and was improving VOCs and by-products conversion. Various publications and reviews give detailed reports on non thermal plasma (NTP) coupled to catalysis on VOCs removal such as trichloroethylene [8, 11-13], benzene [8, 14-16], toluene [8, 17, 18], isopropanol [19-21] and methanol [22-25]. In particular, a significant attention has been brought on manganese oxide based catalysts, owing to their capacities to store oxygen and activate ozone [11, 16, 17, 19, 25-26]. It is also worthy to

mention that plasma-catalytic reactions improved by ozone were vastly investigated. More specifically, the VOCs abatement on MnO_2 and CeO_2 oxides supported on a large panel of materials (Al_2O_3, TiO_2, zeolites) have been studied [27-32].

In this paper, we report the abatement of methanol (considered as a model molecule) by non thermal plasma discharge processing with and without catalyst in post plasma configuration (PPC). The experiments are carried out under specific conditions, implying a low residence time (0.36 s) and low methanol concentration (25-150 ppm). The plasma reactor consists in DBD surface plasma with an innovative configuration that may be extrapolated to industrial scale. The present reactor configuration is the result of optimized work that allows the treatment of high flow rates of pollutants with large ozone production. The results are presented in terms of methanol conversion, by-products formation and ozone concentration as a function of methanol concentration, catalyst nature and deposited energy. A kinetic model is presented and reaction mechanisms are proposed for methanol decomposition without catalyst.

2. Experimental

2.1. Non thermal plasma reactor characteristics and experimental setup

A plasma reactor with a dielectric barrier discharge (DBD) configuration was developed for the decomposition of methanol. The DBD plasma is confined in a Plexiglas case of length 230 mm, width 100 mm and 50 mm height (figure 1). A glass plate of 2 mm thickness (size: 90 x 230 mm) serves as the dielectric material. Copper electrodes are placed on both sides of the dielectric. One of the electrodes is made of a copper tape (Leicester England Advance) of size 50 mm × 50 mm. The other one is a copper comb made of 5 equidistant branches (diameter 2 mm, 50 mm length). A small plexiglass casing, holding the dielectric and the copper comb, is placed in the reactor. It also aims at forcing the gas to flow in a 15 mm gap over the plasma discharge. Sinusoidal high voltage was applied to comb electrode, while the other (copper

tape) was connected to ground. The discharge is initiated between the branches and, depending on the voltage input or frequency, spreads between the branches over the surface. The advantage of such configuration is that it can be easily extrapolated on a larger scale with higher gas flows.

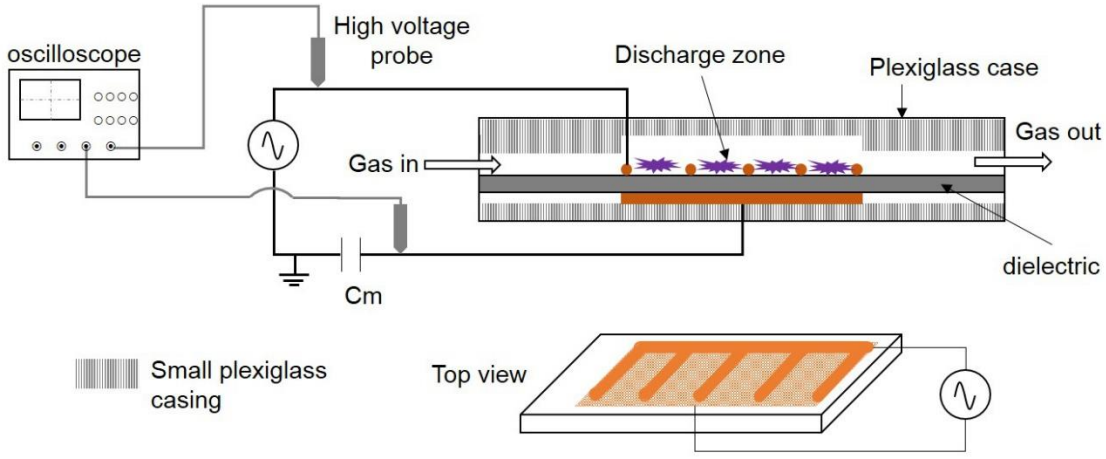

Figure 1: non thermal plasma reactor

The scheme of the overall experimental setup is shown in figure 2. Methanol flow with variable concentrations was adjusted with an automatic evaporation system (Serv'Instrumentation) via the control of different mass flow regulators. High purity N_2 and O_2 gas (Alphagaz 1) were mixed to replicate the composition of air. A constant air flow rate of 5 $L.min^{-1}$ was kept during all the experiments, corresponding to a residence time of 0.36 s in the plasma zone. The different catalysts were hold between two pieces of quartz wool and placed in a glass cylinder tube positioned in post plasma.

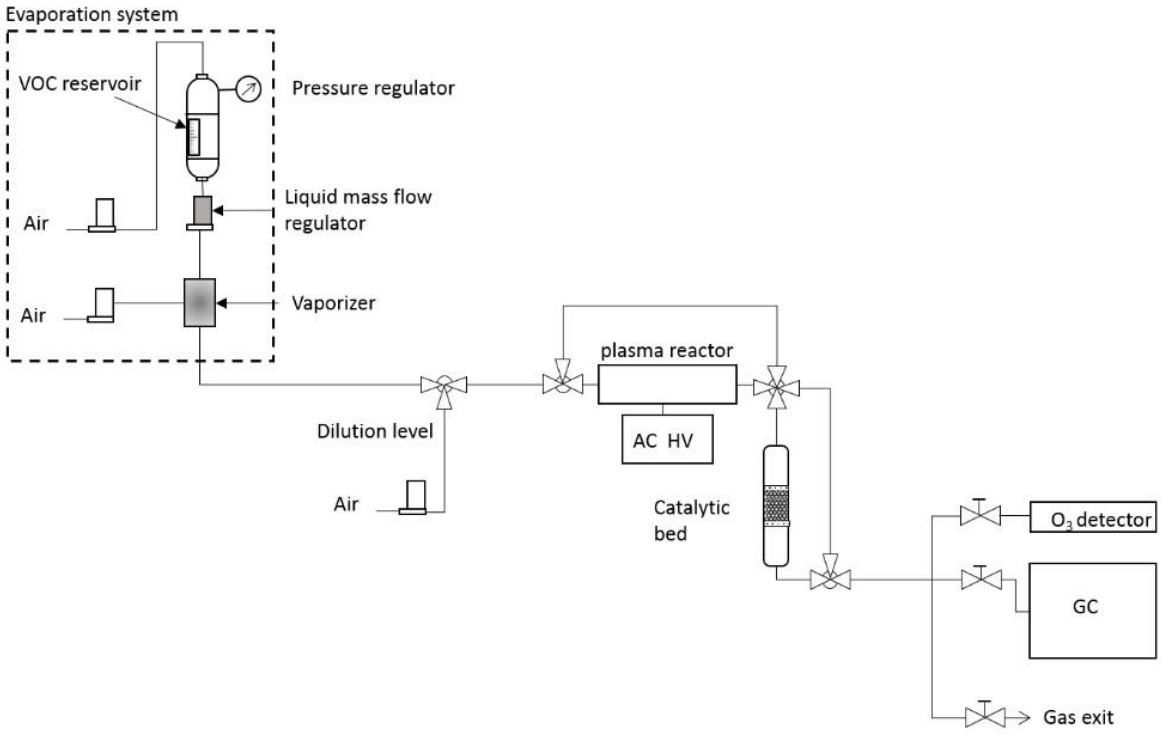

Figure 2: Experimental setup including the evaporation system where liquid methanol is vaporized and diluted in air, plasma reactor and catalyst bed, both fitted with a by-pass.

2.2. Analysis

Calculation of the plasma energy, E_p can be obtained by the Manley method [33] that allows the measurement of the charges, Q across the gas on a capacitance added on the circuit. The parameters that can be measured are the applied voltage, U_a, and the voltage, U_{dbd}, at the capacitance (C_m) terminals. For this purpose, two high voltage probes (Lecroy PPE20KV) were connected, one to the generator output and the second one at the capacitance terminals, respectively. In order to obtain the injected power over one period of time, Lissajous curve, that provides the transferred charge in the reactor, $Q = U_{dbd} \times C_m$ as a function of the applied voltage, U_a, was plotted. The plasma power (P) was then calculated from the multiplication of the frequency (f, in Hz) by the integrated area of the Lissajous parallelogram.

The specific energy density (E_d in $J.L^{-1}$) that links the discharge power to the flow rate (equation 1) is considered as a reference parameter to assess plasma energetic efficiency.

$$E_d = P/F \quad \text{where F is the total flow rate in L.s}^{-1} \text{ (1)}$$

The identification and quantification of gas products, after their contact with the plasma and/or catalyst was determined by online gas chromatography (Perkin Elmer) equipped with a flame ionization detector (FID) and a methanizer. The methanol conversion (X, %) was calculated following:

$$X = \frac{[MeOH]_0 - [MeOH]}{[MeOH]_0} \times 100$$

Selectivities of CO, CO_2 and by-products were calculated from the concentration of identified products, X_p. Calibration curves for each compounds, X_p, were carried out to determine products concentrations.

$$Sel_{X_p}\ (\%) = \frac{[X_p].(number\ of\ C\ of\ X_p)}{[MeOH]_0 - [MeOH]} \times 100$$

The carbon balance, representative of the converted methanol into by-products, CO and CO_2, was determined from the sum of the selectivities:

$$\text{BC } (\%) = \sum Sel_{X_p}$$

All the experiments were reproducible and a margin of error of ± 2 % was calculated. The ozone content was measured with a portable ozone analyzer placed in line (ES, Dualbeam 205).

2.3. Catalyst preparation and characterization

Single metal oxide catalysts of MnO_2/Al_2O_3, CeO_2/Al_2O_3 and CuO/Al_2O_3 were synthesized following the incipient wetness method. γ-Al_2O_3 balls (Axens, 2 mm diameter) were impregnated with an aqueous solution of manganese (II) nitrate tetrahydrate (Riedel-del Haën, 96 %) or cerium nitrate hexahydrate (Ventron, 99.5 %) or copper nitrate trihydrate (Prolabo) with a metal oxide loading of 5 wt.%. The impregnation was carried out under reduced

pressure in a rotary evaporator during 4 h. Water was evaporated by keeping the system at 40 °C for 2 h. The solid was then dried overnight at 110 °C and then calcined under air, during 3 hours at 300 °C for manganese, 400 °C for copper and 600 °C for cerium oxides.

Mixed oxides of MnO_2-CeO_2/Al_2O_3 and MnO_2-CuO/Al_2O_3 were prepared according to the same procedure as described above by successive impregnation. The target loading was close to 5 wt.% for each oxide.

The specific surface area of the samples was determined by the Brunauer–Emmett–Teller (BET) method from the nitrogen adsorption isotherms at −196 °C in an automated Micromeritics Tristar 3000 apparatus after drying for 90 min at 350 °C. The catalysts were characterized by hydrogen temperature programmed reduction (H_2-TPR) using a Micromeritics Autochem 2910 instrument. Samples were pre-treated at 300 °C using high purity helium (50 $mL.min^{-1}$) for 30 minutes. Then H_2 (5 % in Argon) was used as reducing gas with a flow rate of 50 $mL.min^{-1}$. The catalyst was heated up to 600 °C with a temperature rate of 10 $°C.min^{-1}$. The metal oxide loadings were determined by inductively coupled plasma optical emission spectrometry (ICP-OES) using a Perkin Elmer Optima 2000 DV.

3. Results and discussion

3.1. Catalyst Characterization

The prepared catalysts were characterized by BET, ICP and H_2-TPR. The specific surface area, before and after plasma treatment, and metal loading are summarized in table 1.

Table 1 : BET and ICP analysis of the different catalysts

Catalyst	**S_{BET} ($m^2.g^{-1}$)**	**S_{BET} ($m^2.g^{-1}$) After reaction**	**ICP (oxide wt.%)**
γ-Al_2O_3	202	202	-
MnO_2/γ-Al_2O_3	179	207	5
CeO_2/γ-Al_2O_3	178	172	4.7
CuO/γ-Al_2O_3	197	181	3.9
MnO_2-CeO_2/γ-Al_2O_3	177	178	4.5 (CeO_2) 3.8 (MnO_2)
MnO_2-CuO/γ-Al_2O_3	186	168	3.7 (CuO) 4 (MnO_2)

Figure 3 presents the H_2-TPR profiles of the five catalysts. H_2-TPR is a commonly used technique that brings information on the oxidation state of metal oxides and, in this case, of CeO_x and MnO_x phases. The single metal oxides (MnO_2, CeO_2 and CuO) on alumina present one reduction peak which temperature depends on the chemical nature of oxides: 263 °C, 300 °C and 458 °C for CuO/Al_2O_3, MnO_2/Al_2O_3 and CeO_2/Al_2O_3, respectively.

The deposition of a metal oxide led to a slight decrease (up to 12 % for MnO_2-CeO_2/γ-Al_2O_3) of the surface area of the commercial alumina balls. The contact of the catalyst with long-lived species exiting from the plasma reactor did not affect their surface areas, or only by a few percent (max 5 %).

The H_2-TPR profile of MnO_2/Al_2O_3 consists of an asymmetric peak, with a maximum at 300 °C. The curve finishes with a shoulder starting above 350 °C (figure 3a). The fitting of the peak (figure 4) revealed the presence of a second step of reduction with a maximum at 395 °C. According to the literature [19, 34-39], the reduction of MnO_2 to Mn_2O_3/Mn_3O_4 then MnO leads to the formation of 2 peaks in the H_2-TPR profile. The hydrogen consumption

value, measured in this case, is very close to the estimated one that indicates a complete reduction of the sample (table 2). Additionally, the manganese oxide phase depends on the nature of the precursor used during the catalyst preparation. At low loading (≤ 5 %), when a nitrate precursor is used, Mn^{2+} ions are susceptible to diffuse on the surface and stabilize as a MnO_2 phase during calcination. Finally, from EXAFS, Raman and ab initio calculations, it was suggested that the active centers of MnO_x/γ-Al_2O_3 catalysts consisted of four coordinate mononuclear manganese species [39].

The H_2-TPR profile of CeO_2/Al_2O_3 is characterized by a low-intensity and broad consumption curve that starts above 300 °C and reach a maximum at ~460 °C (figure 3a). CeO_2 is known to be reduced at temperatures over 500 °C (700 °C for bulk ceria) and that below this temperature, only the reduction of the upmost layers of Ce^{4+} occurs. The addition of a support decreases the reduction temperature, the value depending on its nature and on the cerium oxide dispersion. From literature data on ceria reducibility, the oxygen loss from TPR results [38, 40] corresponds approximately to one-electron transfer per CeO_2, in accordance with the reduction of Ce^{4+} to Ce^{3+}.

As soon as CeO_2 is deposited over alumina prior to MnO_2, the reduction peak of MnO_2 is shifted to a higher value: maximum at 320°C instead of 280°C without CeO_2. It shows unambiguously that a much stronger interaction between manganese and the support exist in the presence of CeO_2, suggesting a highly dispersed system.

Regarding CuO/Al_2O_3 containing sample (Fig. 3b), the H_2-TPR present an asymmetric peak at 263 °C with a long shoulder that ends at 500 °C. The same peak fitting method as for MnO_2 (Gaussian fitting with Origin software) was carried out and a second peak, less intense (1/3 of main peak area), at 360 °C was evidenced. The intense peak can be attributed to the reduction of CuO_x species, probably highly dispersed and amorphous [38] and the shoulder to a small amount of CuO crystallites. A complete reduction of the sample into metallic Cu was

achieved as it is observed in table 2, from the calculated (10.9 $cm^3.g^{-1}$) and measured (10.2 $cm^3.g^{-1}$) hydrogen consumption required for the reduction. The addition of copper reduced slightly the reduction temperature of MnO_2 from 300 to 272 °C (figure 3b) and increased the intensity of the resulted peak. According to Sager *et al.* [38], the addition of copper oxide stabilizes the manganese oxide in the form of MnO_2, which is then reduced at a lower temperature.

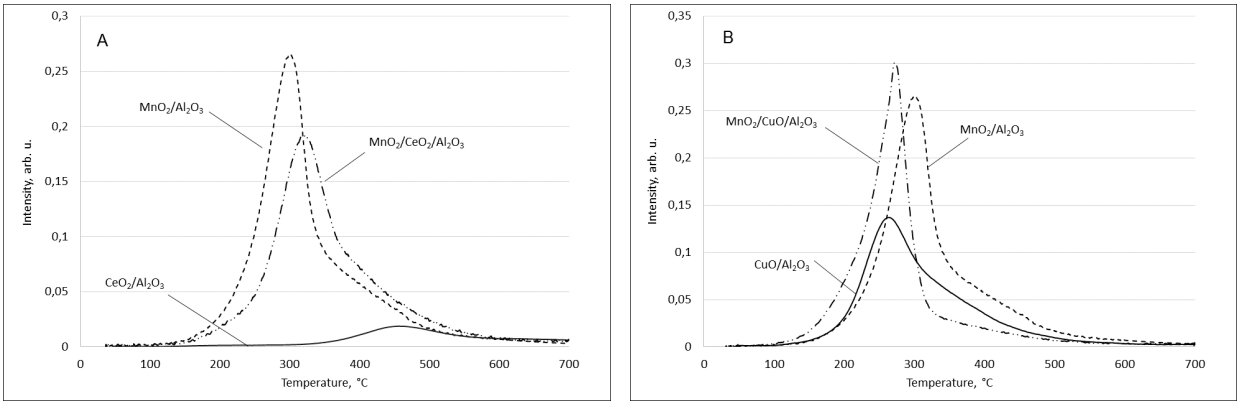

Figure 3: H_2-TPR profiles of the catalysts supported on γ-Al_2O_3. (A): MnO_2 and CeO_2 based catalysts; (B) MnO_2 and CuO based catalysts.

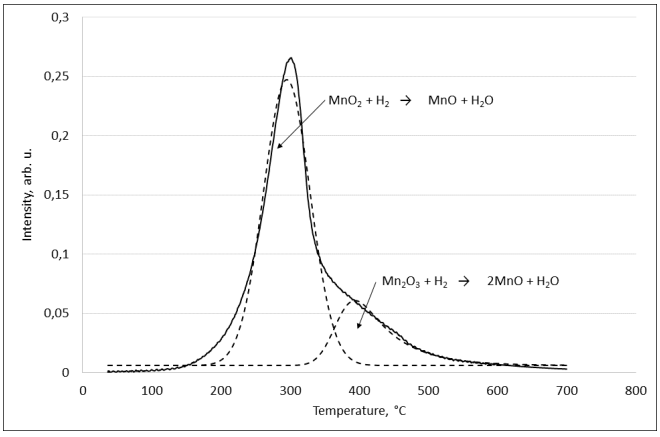

Figure 4: H_2-TPR peak fitting of MnO_2/Al_2O_3 catalyst (Gaussian fitting from Origin software)

Table 2 : H_2-TPR of catalysts: Hydrogen consumption (theoretical and experimental)

Catalyst	Hydrogen consumption for the oxide reduction (cm^3 H_2/g* ± 5 %) STP	
	calculated**	measured***
MnO_2/γ-Al_2O_3	12.9	13.7
CeO_2/γ-Al_2O_3	3.1	2.1
CuO/γ-Al_2O_3	10.9	10.2
MnO_2-CeO_2/γ-Al_2O_3	20.2	23.8
MnO_2-CuO/γ-Al_2O_3	15.7	18.7

*per gram of catalyst;
** calculated from the reduction reactions:
$MnO_2 + H_2 \rightarrow MnO + H_2O$,
$2CeO_2 + H_2 \rightarrow Ce_2O_3 + H_2O$,
$CuO + H_2 \rightarrow Cu + H_2O$;
***obtained from H_2-TPR from integration of the spectra on Origin software.

3.2. Methanol conversion in single plasma configuration

In the single plasma configuration (without catalyst), the methanol conversion increases from 44 % to 75 % with the decrease of the initial concentration of methanol from 150 to 50 ppm (figure 5a) at constant energy input (20 $J.L^{-1}$). These results are in agreement with those from various authors such as Delagrange *et al.* [17] who observed similar behavior for toluene removal from air gas flow.

Non thermal plasma treatment of air leads to the formation of ozone as a main by product [27]. The ozone concentration, remaining unaltered whatever the methanol concentration, indicates that the conversion of methanol does not result from its oxidation by ozone. This behavior is in agreement with various published studies such as that of Harling *et al.* [32] who showed, in the case of toluene and cyclohexane, that ozone cannot directly decompose the

pollutants. Ozone dissociates into oxygen radicals, via its adsorption on the catalyst, which then takes part in the catalytic reaction.

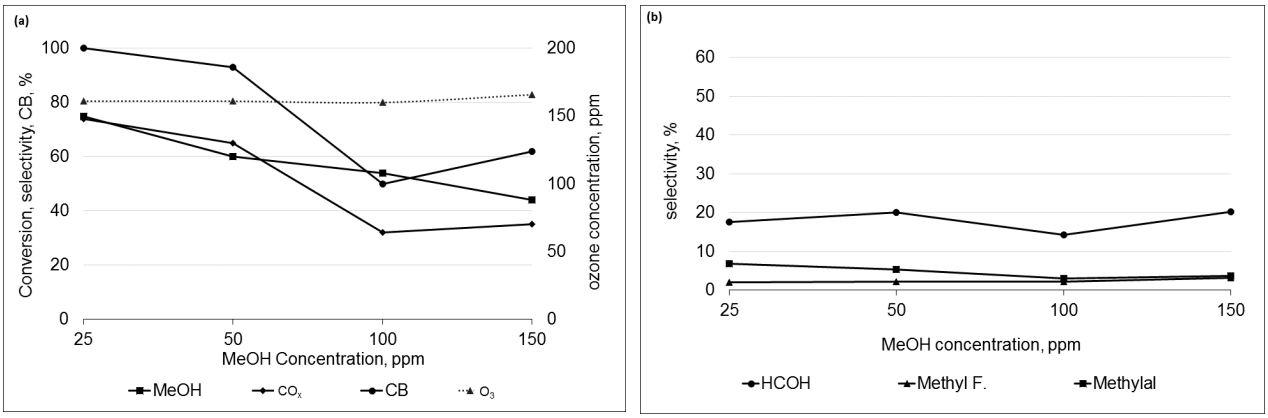

Figure 5: (a) Evolution of methanol conversion, CO_x selectivity ($CO + CO_2$), carbon balance and ozone concentration as a function of the methanol concentration. (b) By-products selectivities as a function of methanol concentration (formaldehyde, methyl formate, methylal). Conditions: energy at 20 $J.L^{-1}$, flow rate 5 $L.min^{-1}$

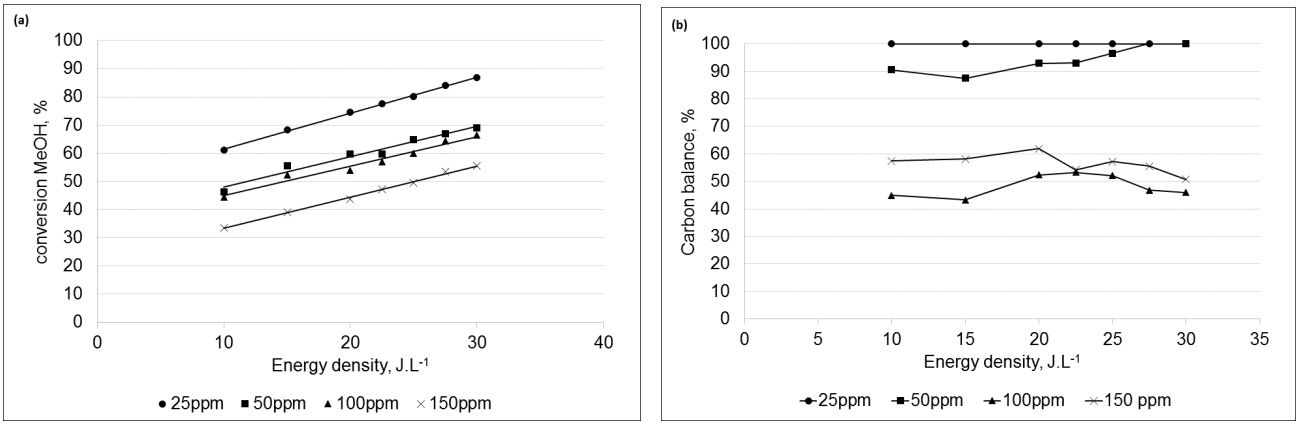

Figure 6: (a) Evolution of methanol conversion as a function of the input energy. (b) Carbon balance at different initial methanol concentration as a function of energy density.

The selectivity to CO_2 does not reach 100 % whatever the methanol concentration. Secondary products were detected and identified as CO, formaldehyde (HCOH), methyl formate ($HCOOCH_3$) and methylal ($CH_3OCH_2OCH_3$). Surprisingly, the carbon balance is not completed for methanol initial concentrations higher than 50 ppm suggesting the formation of

an undetected by-product which could be formic acid resulting from formaldehyde oxidation [41] (see part 3.5).

Methanol conversion increases with the energy density input rise (figure 6a) whatever the methanol initial concentration. The conversion tendency is as expected [17, 20, 42], the lower the methanol initial concentration, the higher the methanol conversion. Different authors [43, 44] explained this tendency via kinetic analysis and proposed that chemical reactions are governed by radical reactions in the plasma discharge.

At 25 ppm, the main products are carbon oxides whose selectivity increases with the energy density (figure 7a). Secondary products are detected with a majority of formaldehyde (25 %) that decreases to 15 % above 20 $J.L^{-1}$. In much less extent, methyl formate (4 %) and methylal (4 %) are generated. Methylal selectivity increases with the energy density (4 to 8 %) while the opposite behavior is observed for methyl formate (4 to 2 %). The same trend is observed at higher methanol initial concentration but with a lower formation of carbon oxides.

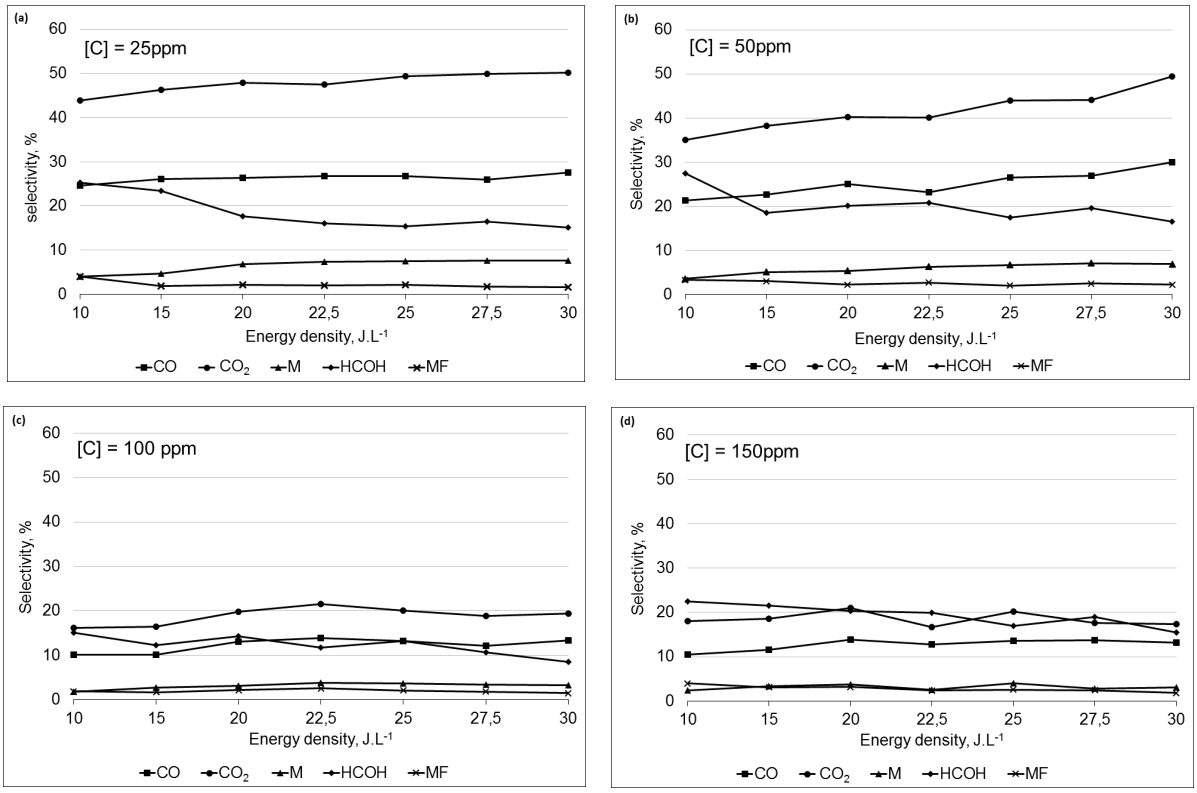

Figure 7: Selectivities to by-products (■ CO, ■ CO_2, ■ formaldehyde, ■ methyl formate and ■ methylal) as a function of the energy density at (a) 25 ppm, (b) 50 ppm, (c) 100 ppm, (d) 150 ppm

These results were compared with published data on methanol, IPA and ethanol abatement with different configurations of non thermal plasma reactors. The list of references given in the table below (table 3) is non exhaustive but gives an overview of different systems aiming at the abatement of various pollutants. In all cases, the conversion results reported here are made without a catalyst. The DBD reactor tested in this study is as efficient, in terms of energy density and pollutant conversion, as some of the other systems published in the literature.

Table 3: Overview of different single NTAP systems.

Plasma type	Pollutant	gas	Flow rate ($L.min^{-1}$)	Residence time (s)	[C] (ppm)	Conversion (%)	Energy density ($J.L^{-1}$)	Energy efficiency ($kJ.mmol^{-1}$)	Refs.
Volumic DBD	methanol	air			400	50 at 120°C	230	27	[23]
						50 at 300°C	60	7	[23]
Volumic DBD	methanol	air	1	0.14	1500	60	560	15	[25]
Volumic DBD	IPA	air	14	6	500	92	300	16	[19]
Surface DBD	acetone	air	8	1.1	50	17	6	17	[29]
Surface DBD	toluene	air	0.5	0.94	200	60	600	120	[30]
Surface DBD	Isovaler-aldehyde	air	10	0.9	50	39	5.4	7	[31]
Surface DBD	toluene	air	5	0.05	200	70	310	53	[41]
	benzene					40	305	92	[46]
Surface DBD	methanol	air	5	0.36	50	60	20	16	This work

According to several authors [47-50] the methanol decomposition by non thermal plasma occurs mainly through radical reactions with formation of formaldehyde, methyl formate and methylal before complete oxidation to carbon oxides. It is important to notify that NOx was not detected at 20 J. L^{-1}.

3.3. Effect of the electrode nature

The effect of the electrode nature was evaluated on the methanol conversion and ozone production. We observed a slight increase, from 44 to 47 %, of the methanol conversion with

stainless steel electrodes instead of copper electrodes (figure 8). In the same time, the ozone concentration decreased from 180 ppm to 166 ppm. It has been already proven that the nature of the electrode affects not only the plasma current-voltage characteristics but also the ozone concentration [50-52]. These authors emphasized the importance of the interaction of ozone with the electrodes and showed that stainless steel electrodes favored ozone decomposition while copper produced higher ozone yield in both positive and negative corona discharges.

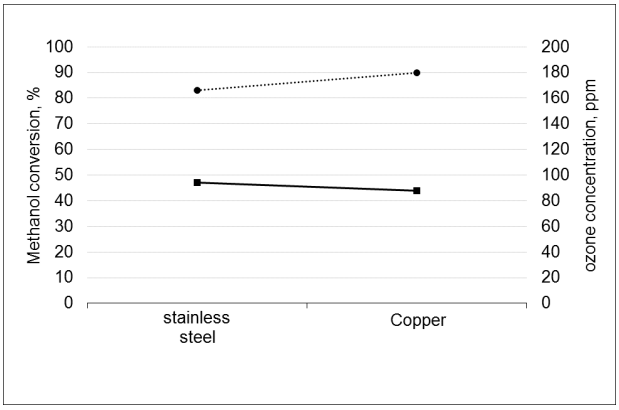

Figure 8: effect of electrode chemical nature on methanol conversion and ozone production

3.4. Kinetic analysis

Yan and Huijbrechts [43] and Rosocha et al. [44] proposed a simplified general kinetic model to provide information on plasma behavior with regard to pollutant removal.

They based their model on four reactions starting with a radical type reaction:

Radical production reaction, k_1 $M \rightarrow R$ (R1)

Pollutant removal reaction, k_2 $C + R \rightarrow A$ (R2)

Radical linear termination reaction, k_3 $R + M \rightarrow B$ (R3)

Radical nonlinear termination reaction, k_4 $R + R \rightarrow C$ (R4)

Where R is radical, C is pollutant, A, B, C are by-products and M are bulk gas compounds.

They suggested that at intermediate energy densities, that is when the radical concentration increases, then radical linear termination reaction (R3) becomes the dominant process and the decomposition of methanol follows the relation:

$$\frac{[C]}{[C_0]} = 1 - X = \exp^{-\frac{E}{\beta}}$$

hence

$$\beta = \frac{-E}{\ln(1-X)}$$

Where [C] and [C_0] are the pollutant and initial pollutant concentrations, E is the energy density ($J.L^{-1}$), X the conversion. β value ($J.L^{-1}$) corresponds to the specific energy. They specified that the energy efficiency of the system may be evaluated by the β value. The smaller the energy cost, the smaller the β value and the higher the removal efficiency. We applied this model to our experimental data and plotted ln (1-X), as a function of the energy density (E) and this for 4 different concentrations. The β values, deduced from the slopes, were then plotted as a function of the square root of the concentration and we obtained a linear correlation between the two parameters:

$$\beta = 2.8\sqrt{[C_0]}$$

Thus,

$$X = 1 - exp^{-E/(2.8\sqrt{[C_0]})}$$

The theoretical calculations fit with the experimental results and are displayed on figure 9. This model is in accordance with results published by Delagrange *and al.* [17] and with Yan *and al.* approximation: the lowest the concentration, the lowest the energy cost of the system and the highest the removal efficiency.

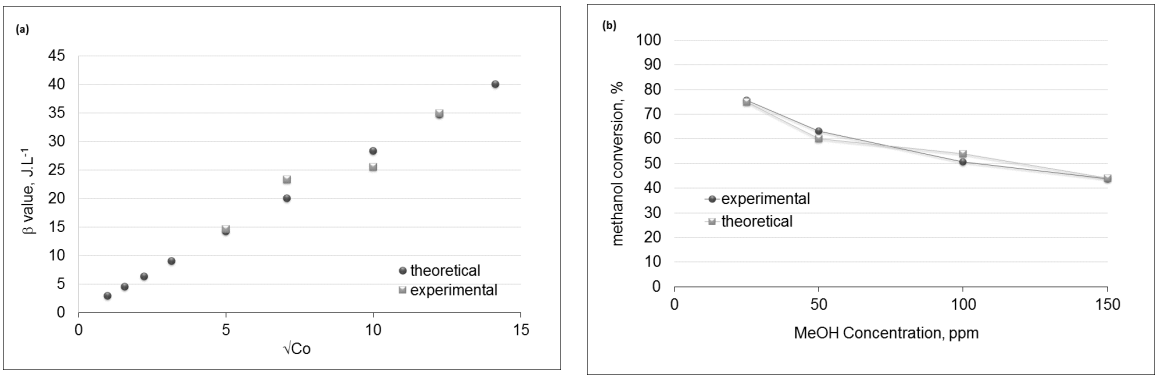

Figure 9 : (a) Variation of the β value as a function of methanol concentration from the model (theoretical) and experimental results (b) methanol conversion from experimental results and model deduced from: $\boldsymbol{X = 1 - exp^{-E/(2.8\sqrt{[C_0]})}}$

The model was extrapolated to higher energy densities for each concentration (figure 10). From these calculations, an energy density of 45 $J.L^{-1}$ is required to reach 95 % conversion at 25ppm initial methanol concentration. This value increases to 70 $J.L^{-1}$ at 50 ppm, 80 $J.L^{-1}$ at 100 ppm and 105 $J.L^{-1}$ at 150 ppm.

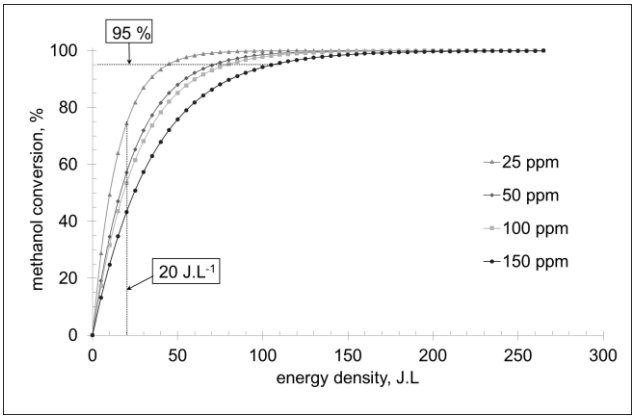

Figure 10: Extrapolation curves of the model as a function of energy density

In order to minimize the energy consumption and make use of the ozone produced by the discharge, a catalyst was placed in post plasma configuration. Ozone is stable up to 250°C

and a catalyst is necessary to trigger its decomposition. Ozone decomposes into active species that can undergo oxidation reactions at the surface of the catalyst.

3.5. Coupling non thermal plasma to catalysis

It is now well-admitted that the addition of a catalyst within the discharge or in the post plasma region is primordial to promote the pollutant conversion and selectivity to CO_2 and H_2O. As mentioned above, MnO_2 and CeO_2 based catalysts have shown very interesting effects when coupled to a plasma discharge. The effect of these metal oxides supported on alumina on methanol conversion is detailed below. Additionally, CuO was deposited on these materials and its influence investigated. The experiments were carried out at an initial concentration of 150 ppm of methanol in a 5 $L.min^{-1}$ flow rate at a constant energy density of 20 $J.L^{-1}$. 1 g of catalyst was placed in the reactor (figure 2) and held between two pieces of quartz wool. The effects of different catalysts in a post discharge configuration were evaluated in terms of methanol conversion, carbon balance, by-products and ozone concentration. The results are displayed in figure 11.

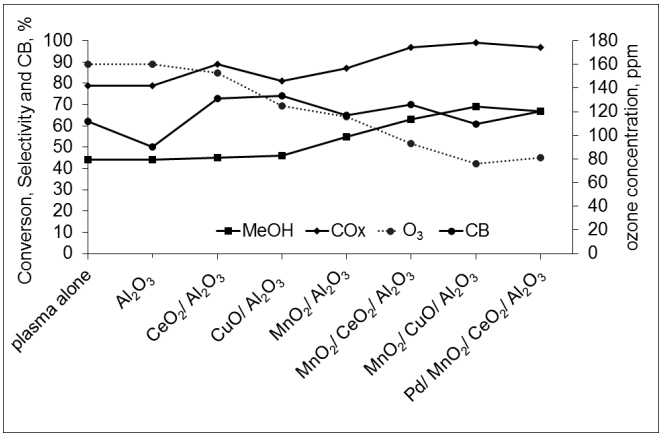

Figure 11 : Evolution of methanol conversion, CO_x selectivity ($CO + CO_2$), carbon balance and ozone concentration as a function of catalyst nature. Conditions: 150 ppm of methanol in a 5 $L.min^{-1}$ air flow at a constant energy density of 20 $J.L^{-1}$ and 1 g of catalyst.

The beneficial effect of the catalysts on methanol conversion is as follow:

$Al_2O_3 \leq CeO_2/ Al_2O_3 \leq CuO/ Al_2O_3 < MnO_2/Al_2O_3 < MnO_2\text{-}CeO_2 /Al_2O_3 < MnO_2\text{-}CuO /Al_2O_3$

Selectivity to CO_x is only improved when CeO_2 is supported on alumina, rising from 35 % (plasma alone) to 44 %. The MnO_2 based catalysts show a slight decrease of CO_x selectivities (30-32 %) while the pure Al_2O_3, CuO and mixed CeO_2-MnO_2 selectivities remain unaltered (34-35 %). CeO_2-MnO_2/ Al_2O_3, CuO/Al_2O_3 and CeO_2/Al_2O_3 catalysts increase the carbon balance up to 70 %, 73 % and 74 %, respectively. When MnO_2-CuO is supported on alumina, the carbon balance does not differ much from single plasma treatment (60-61 %). A little improvement is observed with MnO_2 /Al_2O_3 (65 %). An experiment has been performed with 4 g of MnO_2-CeO_2/Al_2O_3 catalyst in order to test the efficiency of the catalyst on the conversion of methanol. The methanol oxidation reaction was considerably enhanced. Methanol conversion was total for initial concentrations of 100 and 50 ppm and reached 84 % at 150 ppm and the carbon balance was 100 % at any concentration. The selectivity to by-products is shown in Table 4. At 50 ppm, the selectivity to CO and CO_2 was complete, but 23 ppm of ozone was not converted. Compared to plasma alone the high value of methyl formate selectivity for an initial methanol concentration of 100 and 150 ppm strongly suggests that the undetected product is formic acid which could react on the catalyst surface with methanol to form methyl formate through esterification reaction.

Ozone consumption follows roughly the methanol conversion (figure 11) and reaches a maximum for MnO_2-CuO/Al_2O_3 catalyst highlighting the role of ozone as oxidative species on a catalyst.

When looking in more details at the reaction, it was possible to differentiate the activity of the catalyst to secondary products. Methylal selectivity remained low and constant (2-4 %) independently of the catalyst nature whereas methyl formate selectivity increases strongly along with ozone consumption. CO_x selectivity (44%) was the highest when cerium was

present on the catalyst surface. If MnO_2-CuO /Al_2O_3 showed the best ozone abatement and conversion rate, it also favors secondary products formation such as formaldehyde, methyl formate and CO. The increase of by-products selectivities as a function of the oxide nature revealed the catalyst potential to make use of ozone.

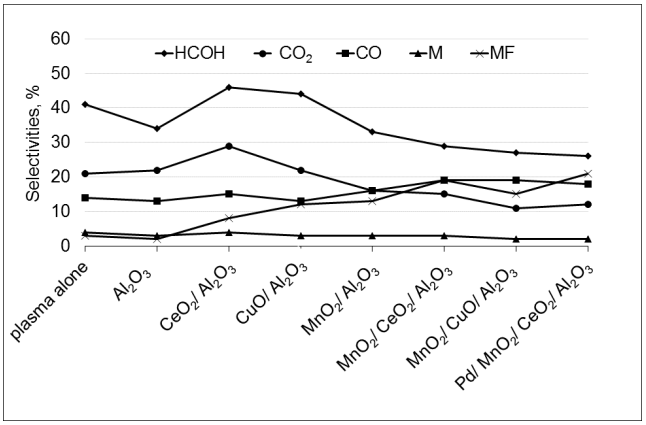

Figure 12 : Evolution of by-products selectivities, CO_x selectivity (CO + CO_2) and ozone concentration as a function of catalyst nature. Conditions: 150 ppm of methanol in a 5 $L.min^{-1}$ air flow at a constant energy density of 20 $J.L^{-1}$ and 1 g of catalyst.

Table 4 : Summary of methanol conversion and by-products selectivities as a function of initial methanol concentration on 4g of MnO_2-CeO_2 /Al_2O_3 catalyst. Conditions: 5 $L.min^{-1}$ air flow and constant energy density of 20 $J.L^{-1}$.

Concentration, ppm	**50**	**100**	**150**
Methanol conversion, %	100	100	84
Carbon balance, %	100	100	100
CO_2 selectivity, %	52	16	10
CO selectivity, %	48	44	42
HCOH selectivity, %	0	5	17
Methyl formate, %	0	35	30
Methylal, %	0	0	1
Ozone concentration, ppm	23	12	12

We have observed that ozone generated by the plasma alone does not participate in the pollutant conversion by gas phase reaction. The presence of a catalyst enhances the methanol decomposition via ozone activation on its surface and its subsequent dissociation into atomic oxygen which then participates in the methanol oxidation reaction.

As observed by several authors [53-55], ozone activation on CeO_2 proceeds by ozone adsorption on Lewis acid site through an electron transfer from Ce^{3+} to O_3 leading to the formation of an instable intermediate ozonide species O_3^- ($Ce^{3+} + O_3 \rightarrow Ce^{4+} + O_3^-$), stabilizing on basic surface sites, which rapidly forms surface peroxide and superoxide ions. At low temperature, these species react with methanol or adsorbed methoxy groups to form formate species prior to CO/CO_2.

The beneficial effect of MnO_2 on ozone activation is very well-known and has been widely investigated [55-67]. The interest comes from two major catalytic properties of MnO_2: 1)

MnO_2 is an oxide presenting different oxidation states; 2) it has an ability to store oxygen. The most reliable point regarding VOC decomposition by ozone concerns the active oxygen species, coming from surface stabilized ozone and responsible for the improved reactivity. In fact, adsorbed ozone species do not remain in molecular form and transform to oxygen species such as O^-, O_3^- and active species such as O (^3P), O (^1D) which show higher reactivity towards VOC abatement than does simply ozone. The active metal oxide sites appear to be Mn^{4+} that is reduced back to Mn^{2+} during desorption of oxygen active species [39, 59]. The ozone decomposition mechanism [60] proposed by Li *and al.* leads to the formation of peroxide and superoxide species.

$O_3 + M^{n+} \rightarrow O_2 + O^- + M^{(n+1)+}$

$O^- + O_3 \rightarrow O_2 + O_2^-$

M = metal site

The formation of superoxide or peroxide with ionic character was also suggested by Oyama *et al.* [39, 55]. They highlighted the importance of the catalyst nature (p-type oxides like MnO_2 and CuO) on ozone decomposition. These active oxygen surface species can not only react with pollutant molecules at the catalyst surface as proposed by Futamura [57], but also improve the selectivity to CO_2 [58-61].

A synergetic effect was observed when CuO or CeO_2 was deposited prior to MnO_2 on alumina. Within the different reported mechanisms, the most recent studies on CuO mixed oxides implied that the improved reactivity towards methanol conversion and ozone abatement is due to reactions occurring at the interphase of the CuO with MnO_2 [25, 62-65]. The catalytic activity was found to be dependent on the perimeter size between CuO and MnO_2. Not only the availability of oxygenated species, but also the couple Mn^{3+} /Mn^{4+} may participate in the reaction. In fact, it was suggested that the redox couple, $Cu^{2+} + Mn^{3+} \rightarrow Cu^+ + Mn^{4+}$ formed on the surface of CuO-MnO_x sample enhances the catalyst reactivity in

oxidation reaction [62]. TPR results showed that addition of copper oxide favors the MnO_2 reduction and then may be responsible for the enhanced activity of $MnO_2/CuO/Al_2O_3$ on the VOC conversion [38].

Regarding cerium oxide based catalysts, Zhu et al. have proposed a mechanism for methanol decomposition on Mn-Ce catalysts. Based on their studies and related published work [25, 61, 68-70], they suggested that Mn loading was the most important parameter affecting the abatement of methanol. The addition of CeO_2, acting as an oxygen release /storage material, led to interactions between Mn and Ce oxides and a synergetic effect was observed, enhancing the oxygen mobility on the catalyst and allowing the deep oxidation of methanol. It is now well established that methanol activation proceeds via its methoxy form adsorbed on the metal oxide surface. Following this step, oxidation into formaldehyde occurs via dehydrogenation (β-H elimination) [71-73]. This reaction is then closely followed by the formation of methyl formate and methylal via O* activation [73**Erreur ! Source du renvoi introuvable.**], with a fraction of these by-products being then desorbed into CO and CO_2. Therefore, the increased presence of formate ions on the surface, that are prone to react with methanol, explains the high methanol conversion and methyl formate selectivity, as observed here.

4. Conclusion

The abatement of methanol during non-thermal plasma discharge processing, under specific conditions implying a low residence time (0.36 s) and specific energy (20 $J.L^{-1}$), led to the conversion of methanol up to 75 % at 25 ppm and 44 % at 150 ppm initial methanol concentration with 160 ppm ozone formation. The plasma reactor consisted in a surface DBD plasma with an innovative configuration that may be extrapolated to industrial scale. By-products were identified as formaldehyde, methyl formate, methylal, CO, CO_2 and ozone. Ozone oxidation properties were activated in the presence of a catalyst in the post discharge

configuration. Three metal oxides, MnO_2, CeO_2, CuO supported on Al_2O_3, were studied. It appeared that bi-metallic oxides of $MnO_2/CeO_2/ Al_2O_3$ and $MnO_2/CuO/Al_2O_3$ presented the best activities in terms of methanol conversion, carbon oxides selectivities and ozone utilization. When 4g of $MnO_2/CeO_2/Al_2O_3$ were used 100 % methanol conversion was obtained with 48 % and 52 % selectivity to CO and CO_2, respectively in a 50 ppm pollutant flow. A synergetic effect was observed with CuO or CeO_2 deposited prior to MnO_2 on alumina and the improved reactivity towards methanol conversion and ozone use could be due to reactions occurring at the interphase of the CuO or CeO_2 with MnO_2. The mechanism could consist in the activation of methanol O-H bonds, forming adsorbed methoxy species on the surface. They decompose first into formaldehyde, then in methyl formate and methylal via O* activation, and finally into CO and CO_2, being desorbed from the surface. Formic acid is produced from the hydrolysis of methyl formate and the increased presence of formate ions on the surface explains the high methanol conversion and methyl formate selectivity.

Acknowledgment

The authors are thankful to the ANRT for the financial support.

References

1. A. Bogaerts, E. Neyts, R. Gijbels, J. Van der Mullen, Gas discharge plasmas and their applications, Spectro. Acta Part B 57 (2002) 609 - 658.
2. P. Attri, B. Arora, E. Ha Choi, Utility of plasma: a new road from physics to chemistry, RSC Adv. 3 (2013) 12540 -12567.
3. C. Tendero, C. Tixier, P. Tristant , J. Desmaison, P. Leprince, Atmospheric pressure plasmas: A review, Spectro. Acta Part B 61 (2006) 2 - 30.

4. U. Kogelschatz, Dielectric-barrier Discharges: Their History, Discharge Physics, and Industrial Applications Plasma Chem. Plasma Process 23 (2003) 1-46
5. U. Kogelschatz, B. Eliasson and W. Egli, From ozone generators to flat television screens: history and future potential of dielectric-barrier discharges, Pure Appl. Chem. 71 (1999) 1819 - 1828.
6. J. Van Durme, J. Dewulf, C. Leys, H. Van Langenhove, Combining non thermal plasma with heterogeneous catalysis in waste gas treatment: A review, Appl. Cat. B: Env. 78 (2008) 324 - 333.
7. K. Hyun- Ha, Non thermal Plasma Processing for Air-Pollution Control: A Historical Review, Current Issues, and Future Prospects, Plasma Process. Polym. 1 (2004) 91 - 110.
8. A.M. Vandenbroucke, R. Morent, N. De Geyter, C. Leys , Non thermal plasmas for non-catalytic and catalytic VOC abatement, J. Haz. Mat. 195 (2011) 30 - 54.
9. G. Xiao, W. Xu, R. Wu, M. Ni, C. Du, X. Gao, Z. Luo, K. Cen, Non thermal plasmas for VOCs abatment, Plasma Chem. Plasma Process. 34 (2014) 1033 - 1065.
10. S. Sultana, A. M. Vandenbroucke, C. Leys, N. De Geyter, R. Morent, Abatment of VOCs with alternate adsorption and plasma assisted regeneration, Catalysts 5 (2015) 718-746.
11. A.M. Vandenbroucke, M. Mora, C. Jiménez-Sanchidrián, F.J. Romero-Salguero, N. De Geyter, C. Leys, R. Morent, TCE abatement with a plasma-catalytic combined system using MnO2 as catalyst, Applied Catalysis B: Environmental 156–157 (2014) 94–100.
12. A. M. Vandenbroucke, M.T. Nguyen Dinh, N. Nuns, J.-M. Giraudon, N. De Geyter, C. Leys, J.-F. Lamonier, R. Morent, Combination of non thermal plasma and Pd/$LaMnO_3$ for dilute trichloroethylene abatement, Chem. Eng. J., 283 (2016) 668-675.
13. Y. Nakagawa, R. Ono, T. Oda, Investigation of Humidity Effect on Atmospheric Plasma Decomposition of Toxic Gas With Direct Optical Measurement of OH Radicals, IEEE Trans. 50 (2014) 39 - 44.

14. J. Karuppiah, E. Linga Reddy, P. Manoj Kumar Reddy, B. Ramaraju, Ch. Subrahmanyam, Catalytic non thermal plasma reactor for the abatement of low concentrations of benzene, Int. J. Environ. Sci. Technol. 11 (2014) 311-318.
15. N. Xu, W. Fu, C. He, L. Cao, X. Liu, J. Zhao, H. Pan, Benzene Removal Using Non thermal Plasma with CuO/AC Catalyst: Reaction Condition Optimization and Decomposition Mechanism, Plasma Chem. Plasma Process. 34 (2014) 1387-1402.
16. Li, Y., Fan, Z., Shi, J., Liu, Z. & Shangguan, W. Post plasma-catalysis for VOCs degradation over different phase structure MnO_2 catalysts. Chemical Engineering Journal 241 (2014) 251 - 258.
17. S. Delagrange, L. Pinard, J.-M. Tatibouët, Combination of a non thermal plasma and a catalyst for toluene removal from air: Manganese based oxide catalysts, Applied Catalysis B: Environmental 68 (2006) 92 – 98.
18. Ch. Subrahmanyama, A. Renken, L. Kiwi-Minsker, Catalytic non thermal plasma reactor for abatement of toluene, Chem. Eng. J. 160 (2010) 677 - 682.
19. J. Jarrige, P. Vervisch, Plasma-enhanced catalysis of propane and isopropyl alcohol at ambient temperature on a MnO2-based catalyst, Appl. Cat B: Env. 90 (2009) 74 – 82.
20. Ch. Subrahmanyam, A. Renken, L. Kiwi-Minsker, Novel Catalytic Dielectric Barrier Discharge Reactor for Gas-Phase Abatement of Isopropanol, Plasma Chem. Plasma Process. 27 (2007) 13–22.
21. L. Sivachandiran, F. Thevenet, P. Gravejat, A. Rousseau, Isopropanol saturated TiO_2 surface regeneration by non thermal plasma: Influence of air relative humidity, Chem. Eng. J. 214 (2013) 17–26.
22. M. Derakhshesh, J. Abedi, H. Hassanzadeh, Mechanism of methanol decomposition by non thermal plasma, J. of Electrostatics 68 (2010) 424-428.

23. M. C. Hsiao, B. T. Merritt, B. M. Penetrante, G. E. Vogtlin and P. H. Wallman, Plasma-assisted decomposition of methanol and trichloroethylene in atmospheric pressure air streams by electrical discharge processing, J. Appl. Phys. 78 (1995) 3451-3456.
24. D. Hoon Lee, T. Kim, Effect of catalyst deactivation on kinetics of plasma-catalysis for methanol decomposition, Plasma Process. Polym. 11 (2014) 455-463.
25. X. Zhu, S. Liu, Y. Cai, X. Gao, J. Zhou, C. Zheng, X. Tu, Post-plasma catalytic removal of methanol over Mn–Ce catalysts in an atmospheric dielectric barrier discharge, appl. Cat. B: Env 183 (2016) 124-132.
26. E. Rezaei, J. Soltan, EXAFS and kinetic study of MnOx/γ-alumina in gas phase catalytic oxidation of toluene by ozone, Appl. Cat. B: Env. 148-149 (2014) 70-79.
27. B. Eliasson, M. Hirth, U. Kogelschatz, ozone synthesis from oxygen in dielectric barrier discharges, J. Phys. D.: Appl. Phys. 20 (1987) 1421-1437.
28. C. Barakat, P. Gravejat, O. Guaitella, F. thevenet, A. Rousseau, Oxidation of isopropanol and acetone adsorbed on TiO_2 under plasma generated ozone flow: Gas phase and adsorbed species monitoring, Appl. Cat. B: Env. 147 (2014) 302-313.
29. A. Maciuca, C. Batiot Dupeyrat, J.M. Tatibouët, Coupling Non thermal Plasma with Photocatalysis for Odorous Pollutants Removal, 8th Int. Symposium on Non Thermal/Thermal Plasma Pollution Control Technology and Sustainable Energy (2012) 135-139.
30. S.M. Oh, H. H Kim, A. Ogata, H. Einaga, S. Futamura, D.W. Park, Effect of zeolite in surface discharge plasma on the decomposition of toluene, Cat. Letters 99 (2005) 101-104.
31. A. Maciuca, C. Batiot Dupeyrat, J.M. Tatibouët, Synergetic effect by coupling photocatalysis with plasma for low VOCs concentration removal from air, Appl. Cat. B: Env. 125 (2012) 432– 438.

32. A. M. Harling, D. J. Glover, J. C. Whitehead, K. Zhang, The role of ozone in the plasma-catalytic destruction of environmental pollutants, Appl Cat B: Env 90 (2009) 157-161.
33. T.C. Manley, The electronic characteristics of the ozonator discharge, Trans. Electrochem. Soc. 84 (1943) 83
34. F. Kapteijn, A.D. Vanlangeveld, J.A. Moulijn, A. Andreini, M.A. Vuurman, A.M. Turek, J.M. Jehng, I.E. Wachs, Alumina supported manganese oxide catalysts, J. Catal. 150 (1994) 94-104
35. F. Arena, T. Torre, C. Raimondo, A. Parmaliana, Structure and redox properties of bulk and supported manganese oxide catalysts, Phys. Chem. Chem. Phys. 3 (2001) 1911-1917
36. L. Wang, H. He, C. Zhang, Y. Wang, B. Zhang, Effects of precursors for manganese-loaded γ-Al_2O_3 catalysts on plasma catalytic removal of o-xylene, Chem. Eng. J. 288 (2016) 406-413
37. Janusz Trawczyński, Beata Bielak, Włodzimierz Miśta, Oxidation of ethanol over supported manganese catalysts – Effect of the carrier, Appl. Cat. B: Env. 55 (2005) 277-285
38. S.M. Saqer, D. I. Kondarides, X.E. Verykios, Catalytic oxidation of toluene over binary mixtures of copper, manganese and cerium oxides supported on γ-Al_2O_3, Appl. Cat. B: Env. 103 (2011) 275-286
39. R. Radhakrishnan, S. T. Oyama, Y. Ohminami, K. Asakura, Structure of $MnOx/Al_2O_3$ Catalyst: A Study Using EXAFS, In Situ Laser Raman Spectroscopy and ab Initio Calculations, J. Phys. Chem. B 105 (2001) 9067-9070
40. H.C. Yao, Y.F. Yu Yao, Ceria in Automotive Exhaust Catalysts Oxygen Storage, J. Catal 86 (1984) 254-265

41. J. M. Tatibouët, H. Lauron-Pernot, Transient isotopic study of methanol oxidation on unsupported V_2O_5. Mechanism of methylal formation, J. Mol. Cat. A: Chem., 171 (2001) 205-216

42. H.H. Kim, S.M.Oh, A. Ogata, S.Futamura, Decomposition of gas-phase benzene using plasma-driven catalyst (PDC) reactor packed with Ag/TiO_2 catalyst, Appl. Cat. B: Env., 56 (2005)213-220

43. K. Yan, E.J.M. van Heesch, A.J.M. Pemen, and P.A.H.J. Huijbrechts, From Chemical Kinetics to Streamer Corona Reactor and Voltage Pulse Generator, plasma chem. Plasma process. 21 (2001) 107-137

44. L.A. Rosocha, R.A. Korzekwa, Advanced Oxidation and Reduction Processes in the Gas Phase Using Non thermal Plasmas, J. Adv. Oxid. Technol. 4 (1999) 247-264.

45. H.H. Kim, A. Ogata, S. Futamura, Oxygen partial pressure-dependent behavior of various catalysts for the total oxidation of VOCs using cycled system of adsorption and oxygen plasma, Appl. Cat. B: Env 79 (2008) 356–367

46. B.M. Penetrante, M.C. Hsiao, J.N. Badsley, B.T. Merritt, G.E. Vogtlin, A. Kuthi, C.P. Burkhart and J.R. Bayless, Identification of mechanisms for decomposition of air pollutants by non thermal plasma processing, Plasma Sources Sci. Technol. 6 (1997) 251-259

47. M. Sugasawa, T. Terasawa, S. Futarama, Additive Effect of Water on the Decomposition of VOCs in non thermal Plasma, IEEE trans. Ind. Appl. 46 (2010) 1692-1698

48. T. Sato, M. Kambe, H. Nishiyama, Analysis of a Methanol Decomposition Process by a Nonthermal Plasma Flow, JSME Int. J. B, 48 (2005) 432-439

49. N. Bundaleska, D. Tsyganov, R. Saavedra, E. tatarova, F.M. Dias, C.M. Ferreira, Hydrogen production from methanol reforming in microwave “tornado”-type plasma Int. J. Hydrogen Energy, 38 (2013) 9145-9157

50. G. Horvath, J. D. Skalny, J. Orszagh, R. Vladoiu, N. J. Mason, Influence of the Outer Electrode Material on Ozone Generation in Corona Discharges, Plasma chem. Plasma process., 30 (2010) 43-53
51. J. A. Souza-Corrêa, C. Oliveira, and J. Amorima, Ozone decay on stainless steel and sugarcane bagasse surfaces, Eur. Phys. J. Appl. Phys. 63 (2013) 11301
52. R. Peyrous, C. Lacaze, Technological parameters that influence the production of ozone in A .D. C. Corona discharge, Ozone Sci Eng 8 (1986) 107-128
53. A. Naydenov, R. Stoyanova, D. Mehandjiev, Ozone decomposition and CO oxidation on CeO_2, J. Mol. Cat. A: Chem. 98 (1995) 9-14
54. K.M. Bulanin, J.C. Lavalley, J.Lamotte, L. Mariey, N.M. Tsyganenko, A.A. Tsyganenko, Infrared Study of Ozone Adsorption on CeO_2, J. Phys. Chem. B 102 (1998) 6809-6818.
55. B. Dhandapani, S.T. Oyama, Gas phase ozone decomposition catalysts, Appl. Cat. B: Env., 11 (1997) 129-166
56. H. Einega, S. Futamura, Catalytic oxidation of benzene with ozone over alumina-supported manganese oxides, J. Cat. 227 (2004) 304-312
57. Futamura, S., Einaga, H., Kabashima, H. & Hwan, L. Y. Synergistic effect of silent discharge plasma and catalysts on benzene decomposition, Cat. Today 89 (2004) 89–95.
58. H. Einaga, S. Futamura, Oxidation behavior of cyclohexane on alumina-supported manganese oxides with ozone, Appl. Cat B: Env 60, 49–55 (2005)
59. V.P. Santos, M.F.R Pereira, M. F. R., J.J.M. Órfão, J.L. Figueiredo, The role of lattice oxygen on the activity of manganese oxides towards the oxidation of volatile organic compounds, Appl. Cat. B: Env 99 (2010) 353–363

60. W. Li, G. V. Gibbs, S. T. Oyama, Mechanism of Ozone Decomposition on a Manganese Oxide Catalyst In Situ Raman Spectroscopy and Ab Initio Molecular Orbital Calculations, J. Am. Chem. Soc. 120 (1998) 9041-9046
61. Y. Wan, X. Fan, T. Zhu, Removal of low-concentration formaldehyde in air by DC corona discharge plasma, Chem. Eng. J. 171 (2011) 314–319.
62. K. Qian, Z. Qian, Q. Hua, Z. Jiang, W. Huang, Structure-activity relationship of CuO/MnO_2 catalysts in CO oxidation, appl. Surf. Sci 273 (2013) 357-363.
63. G. Fortunato, H. R. Oswald, A. Reller, Spinel type oxide for low temperature CO oxidation generated by use of an ultrasonic aerosol pyrolysis process, J. Mater. Chem. 11 (2001) 905-911
64. M.-F. Luo, P. Fang, M. He, Y.-L. Xie In situ XRD, Raman, and TPR studies of CuO/Al_2O_3 catalysts for CO oxidation, J. Mol. Cat. A: Chemical 239 (2005) 243–248
65. F. Severino, J. Brito, O. Carias, J. Laine, Comparative study of alumina-supported CuO and $CuCr_2O_4$ as catalysts for CO oxidation, J. Cat. 102 (1986) 172-179
66. O. D'alessandro, H. J. Thomas, J.E. Sambeth, An analysis of the first step of phenol adsorption-oxidation over coprecipitated Mn-Ce catalysts: A DRIFTS study, Reac. Kinet. Mech. Cat. 107 (2012) 295-309
67. H. Einaga, T. Ibusuki, and S. Futamura, Performance evaluation of a hybrid system comprising silent discharge plasma and manganese oxide catalysts for benzene decomposition, IEEE trans. Ind. Appl. 37 (2001) 1476- 1482
68. C. Doornkamp, V. Ponec, The universal character of the Mars and Van Krevelen mechanism, J. Mol. Cat. A: Chem. 162 (2000) 19-32
69. E. Finocchio, G. Busca, Characterization and hydrocarbon oxidation activity of coprecipitated mixed oxides Mn_3O_4/Al_2O_3, Cat. Today 70 (2001) 213-225.

70. K.R. Phillips, S. C. Jensen, M. Baron, S.-C. Li, C. M. Friend, Sequential Photo-oxidation of Methanol to Methyl Formate on TiO_2(110), J. Am. Chem. Soc., 135 (2) (2013) 574–577
71. C. Houtman, M. A. Barteau, reaction of methanol on Rh(111) and Rh(111)-(2x2)O surfaces: spectroscopic identification of adsorbed methoxide and η^1-formaldehyde, Langmuir 6 (1990) 1558-1566
72. D. R. Mullins, M. D. Robbins, J. Zhou, Adsorption and reaction of methanol on thin-film cerium oxide, Surf. Sci. 600 (2006) 1547–1558
73. J.M. Tatibouët, Methanol oxidation as a catalytic surface probe, Appl. Catal., 148 (1997) 213-252
74. G. T. Whiting, S. A. Kondrat, C. Hammond, N. Dimitratos, Q. He, D.J. Morgan, N. F. Dummer, J. K. Bartley, C. J. Kiely, S. H. Taylor, G. J. Hutchings, Methyl formate formation from methanol oxidation using supported gold palladium nanoparticles, ACS Catal. 5 (2015) 637−644.

Captions list

Tables

Table 1: BET and ICP analysis of the different catalysts

Figures

Figure 9: (a) Variation of the β value as a function of methanol concentration from the model (theoretical) and experimental results (b) methanol conversion from experimental results and model deduced from: $X = -exp^{-E/(2.8\sqrt{[C_0]})}$

Figure 10: Extrapolation curves of the model as a function of energy density

Figure 11: Evolution of methanol conversion, CO_x selectivity (CO + CO_2), carbon balance and ozone concentration as a function of catalyst nature. Conditions: 150 ppm of methanol in a 5 $L.min^{-1}$ air flow at a constant energy density of 20 $J.L^{-1}$ and 1 g of catalyst

Figure 12: Evolution of by-products selectivities, CO_x selectivity (CO + CO_2) and ozone concentration as a function of catalyst nature. Conditions: 150 ppm of methanol in a 5 $L.min^{-1}$ air flow at a constant energy density of 20 $J.L^{-1}$ and 1 g of catalyst